Influence of annealing temperature on crystallite size and optical band gap of LaMnO$_3$ nanocrystallites.

Mohd Abdul Shukur[1,2], K. Vijaya Kumar[1*], G. Narsinga Rao[3]

[1]Department of Physics, JNTUH University College of Engineering Rajanna Sircilla, Agraharam, Rajanna Sircilla - District, 505301, Telangana, India.

[2]Department of Physics, SRR Government Arts & Science College (Autonomous), Karimnagar, 505001, Telangana, India

[3]Department of Physics, Marri Laxman Reddy Institute of Technology and Management, Dundigal, Hyderabad 500043, Telangana, India.

Abstract

Nanocrystalline LaMnO$_3$ perovskite were prepared by combustion method and annealed at 800 and 1000°C for 6 h, The X-ray diffraction (XRD) patterns provided evidence that the structure formed has a Rhombohedral shape and belongs to the $R\bar{3}C$ space group. The XRD peak profile was taken to evaluate average crystallite size, micro strain, dislocation density for both samples. The remarkable growth in the crystallite size, reduction in micro strain and dislocation density was observed with annealing temperature. UltraViolet -visible spectroscopy is used to determine the optical parameters like absorbance, transmittance, reflectance, and refractive index. The optical band gap was measured by the Tauc-plot method and found decreases as function annealing temperature. The observed results of crystallite size and optical band gap are significantly influenced by annealing temperature.

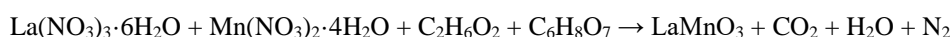* Corresponding author: kvkphd@gmail.com (K. Vijaya Kumar)

1. Introduction

Manganites are a type of mixed oxide composed of manganese that has a perovskite crystal structure and can be represented by the general formula ABO$_3$, where A represents a rare earth element ranging from La to Dy and B represents manganese. One notable characteristic of manganites is their ability to accommodate a wide range of substitutions in their crystal structure. While about 25 elements can occupy the A site, almost 50 different elements can take the place of manganese at the B site. The stoichiometry of manganite corresponds to A^{+3}B^{+3}O$_3$$^{-2}$, with a cubic unit cell that has a body-centered arrangement, where the A^{+3} cation is located at the center of the cell, B^{+3} cations occupy the eight apexes, and O^{-2} anions occupy the midpoints between the cations along the edges of the cell [3-5]. LaMnO3 has a perovskite-like structure consisting of Mn ions surrounded by oxygen atoms, forming MnO6 octahedra with La site cations located between them [6]. LaMnO3, also known as Mott Insulator, exhibits A-type magnetic ordering, where the spins are aligned ferromagnetically within the planes and anti-ferromagnetically between the planes [7]. Manganite compounds usually exhibit a perovskite structure with cubic, orthorhombic, or rhombohedral symmetry depending on the synthesis method as well as the oxygen stoichiometry of LaMnO$_{3-\delta}$ [8-9]. This compound and its solid solutions with alkaline earth elements have been extensively researched due to their potential applications in magnetic insulation and Colossal Magnetoresistance(CMR) technology[10-11].Over the last 20 years, there has been a significant interest in perovskite-structured lanthanum manganite (LaMnO$_3$) due to its unique electronic and magnetic properties, which have potential applications in batteries, pseudo capacitors, and spintronics [12-17]. LaMnO$_3$ has also been found to exhibit catalytic properties and has diverse environmental applications such as oxidation of hydrocarbons, reactions with H$_2$O$_2$, and degradation of chlorinated organic compounds [18-21]. Titanium oxide, on the other hand, is a widely studied semiconductor for photocatalysis due to its low cost, non-toxicity, and high chemical stability, and has a band gap

of approximately 3.2eV. However, most photocatalysts based on wide band gap semiconductors are only active under UV radiation. Thus, there is an urgent need to develop more efficient photocatalytic systems that can operate under visible light irradiation. Perovskite type oxides are promising photocatalysts, but they have limitations such as fast electron-hole recombination, which reduces efficiency. To overcome this, researchers focus on nanocomposites of perovskites, which are advanced materials that have gained increasing attention due to their scientific and technological importance. The properties and functionalities of nanocomposites depend on the composition, atomic order, and size of the aggregates, and the nanoscale regime provides structural and degrees of freedom that are not accessible to bulk materials. Nanocomposite materials that consist of oxides and conducting polymers have found applications in various fields, such as smart windows and photocopying toners. $LaMnO_3$ nanoparticles have attracted significant attention due to their unique optical properties, which are distinct from their bulk counterparts. The optical properties of $LaMnO_3$ nanoparticles are a result of the quantum confinement effect that arises due to the reduced dimensions of the particles. This effect causes a shift in the energy bandgap of the material, resulting in the nanoparticles exhibiting different optical behavior than the bulk material. The understanding of the optical properties of LaMnO3 nanoparticles is crucial for developing these applications. One area of interest for $LaMnO_3$ is its photoconductivity, which refers to the ability of a material to conduct electricity when exposed to light. This property makes $LaMnO_3$ a promising candidate for use in photocatalysis, specifically in the visible light range, which is a critical need for the development of more efficient photocatalytic systems.

Recent studies have not thoroughly investigated the effects of annealing temperatures on the optical properties of $LaMnO_3$ nanocrystallites. Therefore, we present a systematic investigation of the impact of annealing temperature on structural and optical properties such as band gap and optical conductivity of $LaMnO_3$ nanocrystallites. We used the combustion method to prepare the nanocrystallites due to its simplicity, high purity, and ability to control chemical compositions. This method can produce a large quantity of $LaMnO_3$ nanocrystals, even in small amounts[22]. Annealing temperature is known to affect grain size of nanocrystallites, which makes it essential to investigate the influence of annealing temperature on the optical properties of $LaMnO_3$ nanocrystallites to optimize their properties for various applications[23-24]. Our study involved exposing nanocrystallites to annealing temperatures 800 and 1000°C and evaluating different parameters using various analytical devices to gain a comprehensive understanding of how temperature affects the characteristics of $LaMnO_3$ nanocrystallites.

2. Experimental

Nanocrystallites $LaMnO_3$ were synthesized by the combustion method from their nitrate precursors, Lanthanum nitrate $[La(NO_3)_36H_2O]$ and Manganese nitrates $[Mn(NO_3)_2.4H_2O]$ (99% purity AR grade) as reactants using ethylene glycol $(C_2H_6O_2)$, citric acid $(C_6H_8O_7)$ as gelatinizer and chelating agent respectively. The reaction can be represented by the following stoichiometric equation:

$$La(NO_3)_3 \cdot 6H_2O + Mn(NO_3)_2 \cdot 4H_2O + C_2H_6O_2 + C_6H_8O_7 \rightarrow LaMnO_3 + CO_2 + H_2O + N_2$$

The required amounts of lanthanum nitrate, manganese nitrate, in stoichiometric proportions are weighed and dissolved in a small volume of deionized water in a separate beaker. The stoichiometric volume of ethylene glycol and citric acid are added slowly to the nitrate solution with constant stirring. The citric acid, ethylene glycol, and metal nitrate were mixed in a molar ratio 4:3:1. The pH value of the mixed solution was adjusted to 7.0 by adding a small amount of ammonia, obtaining a pink solution. This mixed solution was heated continuously about 80°C with constant stirring on the magnetic stirrer until H_2O evaporation and formation of a glutinous gel. During the dehydration process, poly-condensation reaction happened between citric acid and nitrates, which leads to formation of mentioned gel. The gel was put in an oven at 120°C during 12 hrs, continue heating until all the carbonaceous matter is burned off and the black residue turns into a powdery, grey ash. The gel is continuously heated at around 300°C until the ignition started. Once the gels were ignited and burnt in a self- propagating combustion manner until all gels were completely burnt out to form a loose porous product[25]. This is the combustion process that produces a lot of heat and gas. Finally, the LaMnO3 powder is obtained by annealing the dried ash at a temperature of 800°C and 1000°C for 6 hours in a muffle furnace. This resulted in the production of $LaMnO_3$ nanocrystals with varying sizes. Next, the annealed powders were thoroughly mixed with 1.5% PVA, which acted as a binder, and pressed into pellets using a pressure of 5 tons per cm^2. The pellets were then 10mm in diameter and 2-3mm in thickness. For a duration of four hours, the pellets underwent annealing at both 800°C, and 1000°C.

The X-ray powder diffractometer with Cu Kα incident radiation with wavelength of 1.5418 °A was utilized to determine the phase identification and crystallite size of the $LaMnO_3$ nanocrystals. A Rigaku (Miniflex-II) diffractometer with a step size of 0.02 degrees in the 2theta (20-80) angular range was employed. UV-Vis spectroscopy (SYSTRONICS DOUBLE BEAM) was utilized to assess the optical parameters. The optical

absorbances were acquired by ultrasonic assisted by dispersing a small quantity of sample in distilled water and the data was captured in the range of 200-800nm.

3 Result and Analysis

3.1 XRD Analysis:

The pattern of XRD of $LaMnO_3$ nanocrystallites annealed at 800°C (sample code LMO8), and 1000°C (sample code LMO10) were shown in the figure 1, which shows in good agreement with the diffraction patterns indexed with the JCPDS # 00-082-1152. Theses observed diffraction peaks confirmed the formation of single-phase crystalline nature of rhombohedral structure $R\bar{3}C$ (167) space group without any impurities. The Williamson-Hall (W-H) plot method was employed to accurate determination of the crystallite size and micro-strain present in the sample. The W-H plot relates the Full Width at Half Maximum (FWHM) of the XRD peak to the crystallite size (D) and micro-strain (ε) using a mathematical equation [26].

$$\beta\cos\theta = \frac{0.9\,\lambda}{D} + 4\varepsilon\,\sin\theta \;\ldots\ldots\ldots\ldots\ldots\ldots\ldots (1)$$

where λ is the wavelength of CuKα radiation, β is full width at half maxima (FWHM) in radians, and θ is the Bragg's angle corresponding to the XRD peak, ε is the micro-strain. Figure 2 shows the W-H plot for the samples that were annealed at different temperatures. The W-H plot method involves plotting $\beta\cos\theta$ against $4\sin\theta$ and extrapolating the linear portion of the curve to zero. The experimental data was fitted with a linear equation. The crystallite size and micro-strain of the annealed sample were determined using the intercept on the x-axis and the slope of the linear curve, respectively. Table 1 shows the values of the crystallite size and micro-strain obtained using the W-H plot. It was found that the crystallite size increased from 24.62 to 28.8nm as the annealing temperature was increased from 800°C to 1000°C. On the other hand, the micro-strain decreased with increasing annealing temperature. This can be attributed to the fact that as the annealing temperature increases, the system becomes more crystallized and therefore the micro-strain in the system decreases. Additionally, it was observed that as the annealing temperature increased, the diffraction peak became sharper, indicating an increase in crystallization. The crystal defects in the $LaMnO_3$ nanocrystallites can be measured by the dislocation density(δ_D), which was measured from Williamson and Smallman's relation given by equation (2)

$$\delta_D = \frac{1}{D^2} \;\ldots\ldots\ldots\ldots\ldots\ldots (2)$$

The values of δ_D is shown in Table 1. From this, dislocation density reduces from LMO8 to LMO10 sample due to increase in the crystallite size.
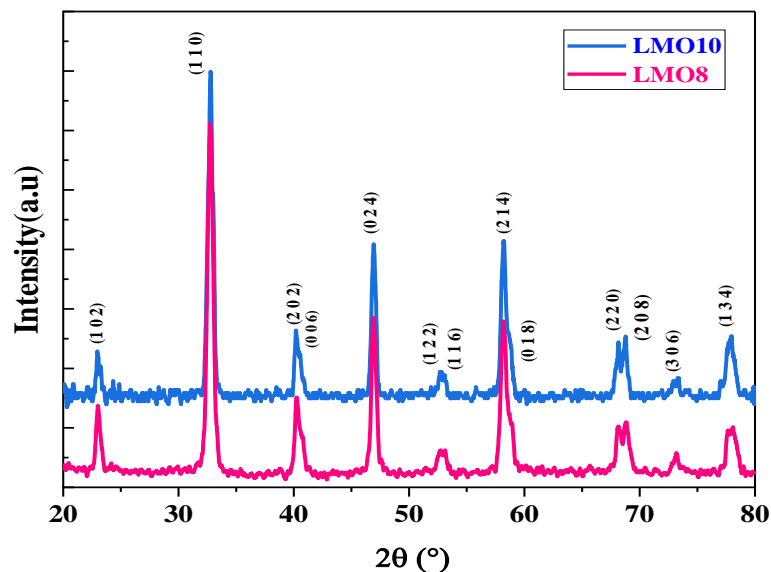

Figure 1: XRD pattern of $LaMnO_3$ nanocrystallites annealed at 800°C (LMO8) and 1000°C (LMO10).
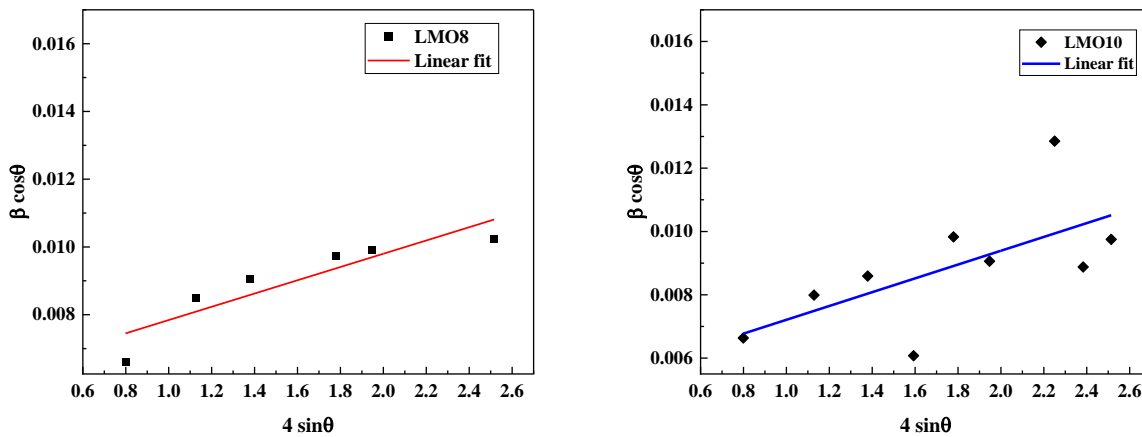
Figure 2: Williamson Hall plot of LaMnO₃ nanocrystallites annealed at 800°C (LMO8) and 1000°C (LMO10).

Table 1: Structural and Optical parameters of LaMnO₃ nanocrystallites annealed at 800°C (LMO8) and 1000°C (LMO10).

Sample code	LMO8	LMO10
Crystallite Size D (nm)	24.62	28.8
Dislocation density (δ_D) (nm^{-2})×10^{-3}	1.6	1.2
Microstrain (ε)×10^{-3}	2.18	1.99
Absorption peak(nm) in UV range	224	231
Absorption peak(nm) in Visible range	448	415
Band gap (eV)	3.46	3.04

3.2 UV-Vis Spectroscopic Analysis

UV-Vis absorption spectra of LMO8 and LMO10 were measured in the range of wavelength 200-800nm to describes the behaviour of optical band gap, refractive index and optical conductivity as a variation of annealing temperature. The variation of absorbance of post annealed LaMnO₃ nanocrystallites with the wavelength was shown in the figure 3(a). It reveals that absorption band identified at 224 and 231nm in the UV range and maximum absorption band at 445 and 415nm in the visible range for the LMO8 and LMO10 respectively.
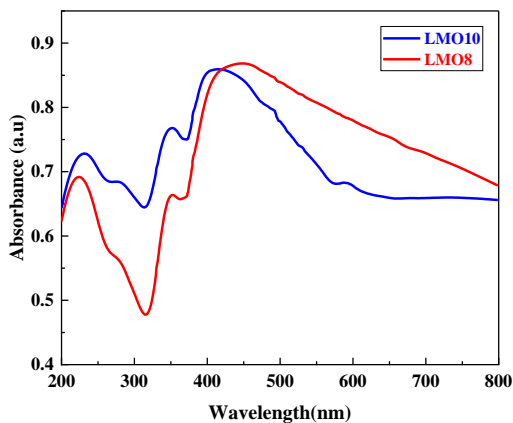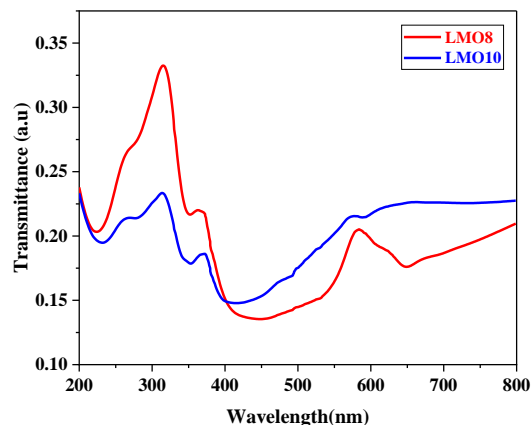

Figure 3(a)

Figure 3(b)

Figure 3(a-b): UV-Vis absorbance spectra and transmittance spectra of LaMnO₃ nanocrystallites annealed at 800°C (LMO8) and 1000°C (LMO10).

Beer- Lambert's Law (3) and (4-5) were used to calculate the absorption coefficient of LaMnO$_3$ nanocrystallites [27-28].

$$I = I_0 e^{\propto t} \ldots\ldots\ldots\ldots\ldots. (3)$$

$$A = log \frac{I_0}{I} \ldots\ldots\ldots\ldots\ldots.. (4)$$

$$\alpha = \frac{2.303 \, A}{t} \ldots\ldots\ldots.. (5)$$

Where $I_0 \rightarrow$ the intensity of incident radiation, $I \rightarrow$ the intensity of transmitted radiation, $\alpha \rightarrow$ the absorption coefficient, $A \rightarrow$ the absorbance, $t \rightarrow$ the thickness of the sample.

Transmittance (T_s) and Reflectance(R) spectra are useful to understand the band structure and energy gap of nano crystallites. Transmittance (I/I_0) and reflectance of LaMnO$_3$ nanocrystallites is given by below relations.

$$T_s = 10^{-A} \times 100 \ldots\ldots\ldots\ldots\ldots. (6)$$

$$R = \frac{(n-1)^2}{(n+1)^2} \ldots\ldots\ldots\ldots\ldots\ldots\ldots. (7)$$

From figure 3(b), high transmittances were observed at 315nm in the UV region for both LMO8 and LMO10 crystallites respectively, which are transparent materials for the optoelectronic devices. The transmittance decreased near 230nm may be due to oxygen vacancies produced.
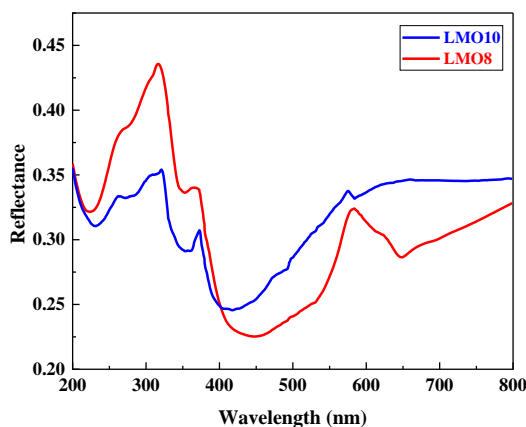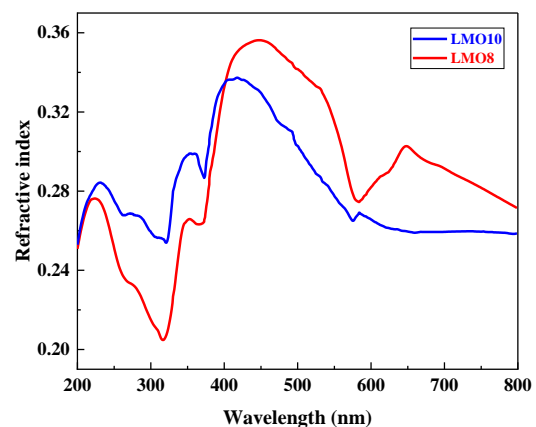

Figure 4(a)　　　　　　　　　　　　Figure 4(b)

Figure 4(a-b): Reflectance and Refractive index spectra of LaMnO$_3$ nanocrystallites annealed at 800℃ (LMO8) and 1000℃ (LMO10).

Refractive index (n) values as a function of wavelength useful to make devices with good optical characteristics. The dynamic refractive index values of LaMnO$_3$ nanocrystallites were evaluated by the relation (8).

$$n = \frac{1}{T_s} + \sqrt{\frac{1}{T_s - 1}} \ldots\ldots\ldots\ldots\ldots\ldots. (8)$$

Variation of reflectance and refractive index with wavelength of LaMnO$_3$ nanocrystallites were shown in the figure 4(a & b). The reflectance value increases from 220-330nm region and attains a maximum value around 420-455nm and decreases in the visible range. It has been noticed that the refractive index values of both samples decrease in the range 220-330nm, then after increases. The maximum refractive index value 0.35 was observed at 446nm for the photon energy 2.78eV for LMO8 and 0.33 at 416nm for the photon energy 2.99eV for LMO10. The enhance in the refractive index is due to the reduction in the porosity of surface of the of LaMnO$_3$ nanocrystallites.

"The extinction coefficient is a measure of light absorption that occurs when the wavelength of the photon is greater than or equal to the size of the grain" [29]. The extinction coefficient of LaMnO$_3$ were evaluated by the absorption coefficient using the relation (9) [30]

$$k = \frac{\alpha\lambda}{4\pi} \ldots \ldots \ldots \ldots \ldots \ldots \ldots (9)$$

where 'k' represents extinction coefficient, and 'α' is the absorption coefficient.

It was observed from the figure 5, the extinction coefficient of both samples increases nonlinearly with the annealed temperature.
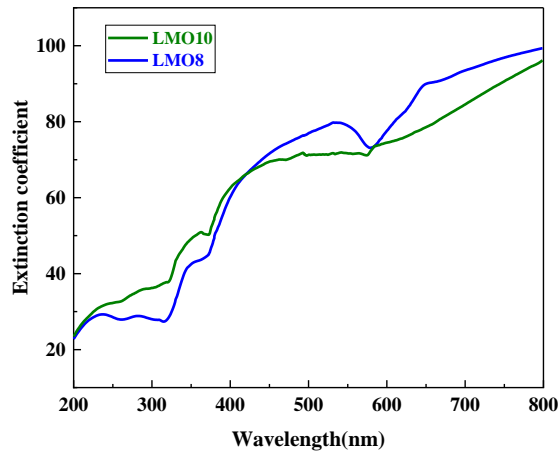

Figure 5: Variation of extinction coefficient as function of wavelength of LaMnO$_3$ nanocrystallites annealed at 800°C (LMO8) and 1000°C (LMO10).

"One of the material's main inherent properties is its real and imaginary dielectric constant. The imaginary component of dielectric constant(ε_i) depicts the absorption of energy (dissipated energy) from the incident electric field owing to dipole motion, whereas the real component(ε_r) shows stored energy. The ratio of real to imaginary components gives the value of loss factor. The imaginary part and real part known by below relations" (10,11) [31-32].

$$\varepsilon_i = 2nk \ldots \ldots \ldots \ldots \ldots \ldots \ldots (10)$$

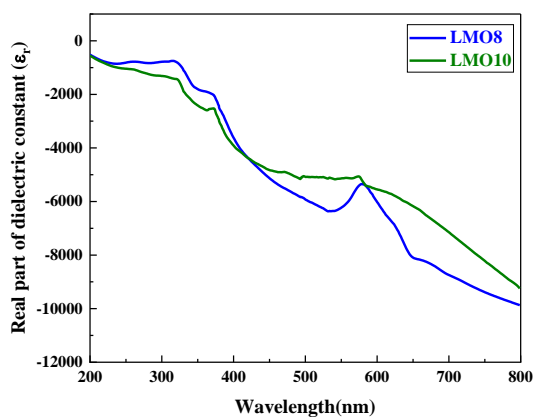$$\varepsilon_r = n^2 - k^2 \ldots \ldots \ldots \ldots \ldots \ldots \ldots (11)$$
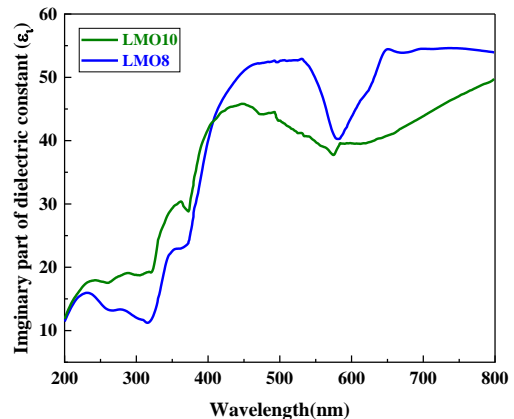

Figure 6(a)

Figure 6(b)

Figure 6: Variation real and imaginary part of dielectric constant as function of wavelength of LaMnO$_3$ nanocrystallites annealed at 800°C (LMO8) and 1000°C (LMO10).

It was noticed from the figure 6(a-b), For the LaMnO3 nanocrystallites, the real dielectric constant (ε_r) values decreases while the imaginary part of dielectric constant (ε_i) increase in a nonlinear manner with increasing wavelength.

The electrical properties of a material can be described by measuring the energy gap value, an energy region where the density of state of electrons was absent. The Tauc plot approach is employed to evaluate the energy gap for known values of absorption coefficient (α), which requires only UV-Vis absorbance data. According to the Tauc, the optical band gap of post annealed LaMnO$_3$ nanocrystallites were calculated using the relation (12)

$$(\alpha h \nu)^n = A\left(h\nu - E_g\right) \dots\dots\dots\dots\dots\dots. (12)$$

where h= Plank's constant (4135×10^{-15}eV.s), ν = frequency (s^{-1}), A= a comparative constant, E$_g$= optical energy gap (eV), 'n' indicates the type of electronic transition [33]. The Tauc plots of ($\alpha h\nu$)^2 as function of photon energy (hν) were plotted. The plot yields an irregular curve but there is a linear part region. In accordance with the equation (12), the value of E$_g$ must be proportional to the value of ($\alpha h\nu$)^2. The linear part is extrapolation is carried out so that it intersects the 'hν' axis. Table 1 presents the direct band gap values of LMO8 and LMO10 nanocrystals, indicating that the optical gap decreased from 3.46 to 3.04eV with increasing annealing temperature. The decrease in the band gap towards lower frequency side attributed to the increase in particle size, as evidenced by the XRD results. The nanocrystals that were prepared are considered promising candidates for photocatalytic applications, as they have appropriate band gap energy values.
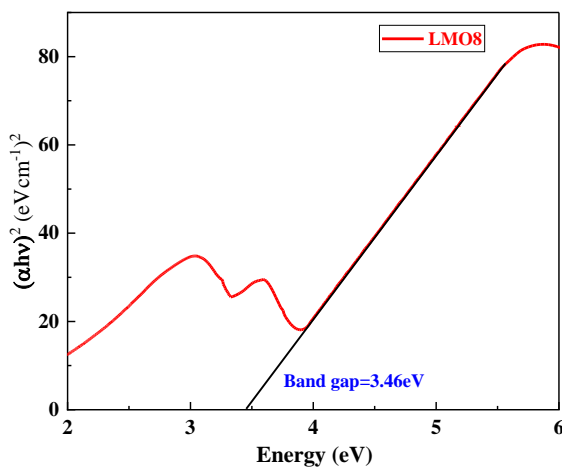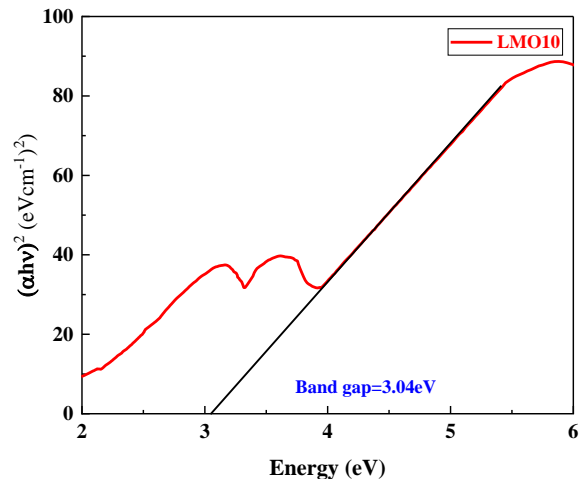

Figure 7(a)

Figure 7(b)

Figure 7(a-b): UV-Vis absorbance -Tauc plot: Variation of ($\alpha h\nu$)^2 versus photon energy 'hν' of LaMnO$_3$ nanocrystallites annealed at 800°C (LMO8) and 1000°C (LMO10).

The skin depth (χ) represents decrease in the amplitude of the incident wave to 1/e after travelling through the distance, which is given by the relation (13) [34].

$$\chi = \frac{1}{\alpha} \dots\dots\dots\dots\dots\dots (13)$$

The skin depth as a function of photon energy is displayed in the figure 8(a), shows that skin depth is maximum value of 0.96µm at photon energy 3.93eV and 0.67µm at 3.87eV for the LMO8 and LMO10 sample respectively.

The optical conductivity (σ) gives information about energy of the photon that can penetrate through the lattice of LaMnO$_3$ nanocrystallites, can be measured by the relation (14).

$$\sigma = \frac{\alpha n c}{4\pi} \dots\dots\dots\dots\dots.. (14)$$
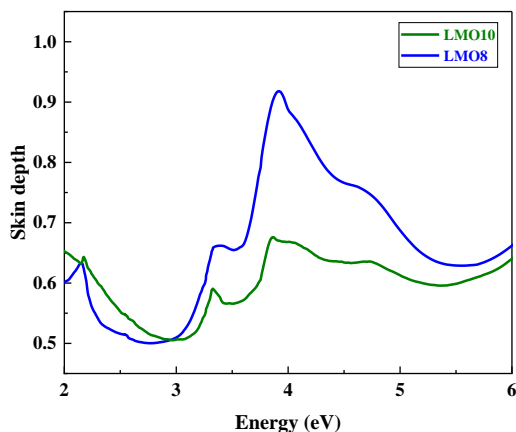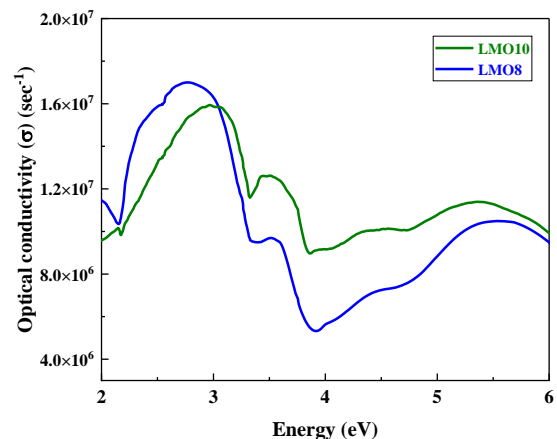
where c is the speed of light.

| Figure 8(a) | Figure 8(b) |

Figure 8(a): Variation of Skin depth and Figure 8(b): Variation of optical conductivity as function photon energy of LaMnO$_3$ nanocrystallites annealed at 800°C (LMO8) and 1000°C (LMO10).

The optical conductivity of a material is a measure of the quantity of free charges it contains. Figure 8(b) shows the variation of optical conductivity as a function of photon energy, and it was observed that for the sample LMO8, the optical conductivity increases in the UV region and reaches a maximum value of 1.69×10^7 at a photon energy of 2.76eV. Similarly, for the sample LMO10, the optical conductivity also increases in the UV region, with a maximum value of 1.59×10^7 at a photon energy of 2.96eV.

4. Conclusions

The combustion method was successfully used to synthesize LaMnO$_3$ nanocrystals The XRD confirmed the formation of a Rhombohedral structure with space group $R\overline{3}C$. As the annealing temperature increased, the crystallite sizes of the LaMnO$_3$ nanocrystals increased from 24.62 to 28.8nm, while the micro strain decreased from 2.18×10^{-3} to 1.99×10^{-3}, and the dislocation density decreased from 1.6×10^{-3} nm^{-2} to 1.2×10^{-3} nm^{-2}. Both samples had maximum absorbance and transmittance bands observed in the absorbance and transmittance curves. The reflectance value increased in the 220-330nm region, reached a maximum value around 420-455nm, and then decreased in the visible range. For the photon energy 2.78eV, the maximum refractive index value of 0.35 was observed at 446nm for the LMO8 sample, and for the photon energy 2.99eV, the maximum refractive index value of 0.33 was observed at 416nm for the LMO10 sample. According to the UV-vis spectroscopic studies, the optical band gap values changed from 3.46eV to 3.04eV as the crystallite size increased, indicating that the LaMnO$_3$ nanoparticles were semiconductor in nature. The optical conductivity increased in the UV region for both samples, with the sample LMO8 reaching a maximum value of 1.69×10^7 for photon energy 2.76eV, and the sample LMO10 reaching a maximum value of 1.59×10^7 for photon energy 2.96eV.

References

[1] Levy, M.R., 2005, Tesis Doctoral Departamento de Materiales ,Universidad de Landres.

[2] Romaguerra Barcelay, Y.,2012, Tesis Doctoral en Fˊısica., Universidad de Porto 2012.

[3] Varshney,D., Kaurav,N., 2004, "Analysis of low temperature specific heat in the ferromagnetic state of the Ca-doped manganites", Eur. Phys. J. B, 37 , pp. 301-309.

[4] Ghosh, S., Sharma A,D., Basu, R.N., Maiti, H.S., 2007 " Synthesis and magnetic characterization of LaMnO3 nanoparticles", J. Am. Ceram. Soc. pp.3741 - 3747.

[5] Fernandez, F., Tesis Doctoral en Quˊˊımica., 2000, Universidad de Santiago de Compostela.

[6] Van Tendeloo, G., Lebedev, O. I., Hervieu, M., & Raveau, B. 2004, "Structure and microstructure of colossal magnetoresistant materials", Report on Progress in Physics, 67, pp.1315-1365.

[7] Murakami, Y., Hill, J.P., Gibbs, D., Blume, M., Koyama, I., Tanaka, M., Kawata, H., Arima, T., Tokura, Y., Hirota, K., & Endoh, Y., 1998, " Resonant X-Ray Scattering from Orbital Ordering in LaMnO3", Physical Review Letter, 81, pp.582-585.

[8] Töpfer, J., & Goodenough, J. B., 1997, "LaMnO3+δ Revisited", Journal of Solid State Chemistry, 130(1), pp.117-128.

[9] Atsumi, T., Ohgushi, T., Namikata, H., and Kamegashira, N., 1997, "Oxygen nonstoichiometry of LnMnO3−δ (Ln=La, Pr, Nd, Sm and Y)". Journal of Alloys and Compounds, 252(1-2), pp.67-70.

[10] Kobayashi, M., Tamura, H., Nakano, H., Satoh, H., & Kamegashira, N., 2008, "Stability of phases in (Ba, Gd) MnO₃ solid solution system", Journal of Rare Earths, 26(2), pp.233-236.

[11] Mahesh, R., Mahendiran, R., Raychaudhuri, A. K., and Rao C. N. R., 1995, "Effect of the internal pressure due to the A-site cations on the giant magnetoresistance and related properties of doped rare earth manganites Ln1-XAXMnO3 (Ln=La, Nd, Gd, Y; A=Ca, Sr, Ba, Pb)", Journal of Solid State Chemistry, 120, 160.

[12] Gibert, M., Zubko, P., Scherwitzl, R., Iniguez, J., Triscone, N.,2012, "Exchange bias in LaNiO3-LaMnO3 superlattices", Nat. Mater, 11, 195.

[13] Mefford, J.T., Hardin, W.G., Dai, S., Johnston, K.P., Stevenson, K.J, 2014, "Anion charge storage through oxygen intercalation in LaMnO3 perovskite pseudocapacitor electrodes", Nat. Mater, 13, pp.726.

[14] Rivero, P., Meunier, V., Shelton, W., 2016 "Uniaxial pressure-induced half-metallic ferromagnetic phase transition in LaMnO₃", Phys. Rev. B, 93, 094409.

[15] Yamada, H., Ogawa, Y., Ishii, Y., Sato, H., Kawasaki, M., Akoh, H., Tokura, Y., 2004, "Engineered Interface of Magnetic Oxides", Science. 305, pp.646.

[16] Yu, K., Yang, S., He, H., Sun, C., Gu, C., Ju, Y., 2009 "Visible light-driven photocatalytic degradation of rhodamine B over NaBiO3: pathways and mechanism", J. Phys. Chem. A. 113(37), pp.10024-32.

[17] Yuasa, M., Nishida, M., Kida, T., Yamazoe, N., Shimanoe, K., 2011 "Bi-Functional Oxygen Electrodes Using LaMnO₃/LaNiO₃ for Rechargeable Metal-Air Batteries", J. Electrochem. Soc. 158, A605.

[18] Moura, F.C., Araujo, M.H., Ardisson, J.D., Macedo, W.A., Albuquerque, A.S., Lago, R. M., 2007, "Investigation of the solid state reaction of LaMnO3 with Feº and its effect on the catalytic reactions with H2O2", J. Braz. Chem. Soc. 18, pp.322.

[19] Nagaraja, R., Kottam, N., Girija, C., Nagabhushana, B., 2012, "Photocatalytic degradation of Rhodamine B dye under UV/solar light using ZnO nanopowder synthesized by solution combustion route", Powder Technol. 215, 91.

[20] Popa, M., Frantti, J., Kakihana, M., 2002, "Lanthanum ferrite LaFeO₃₊d nanopowders obtained by the polymerizable complex method", Solid State Ionics. 154, pp. 437-445.

[21] Yi, N., Cao, Y., Su, Y., Dai, W.-L., He, H.-L., Fan, K.-N., 2005, "Nanocrystalline LaCoO₃ perovskite particles confined in SBA-15 silica as a new efficient catalyst for hydrocarbon oxidation", J. Catal. 230, pp.249-253.

[22] Bokov, D.; Jalil, A. T.; Chupradit, S.; Suksatan, W.; Ansari, M. J.; Shewael, I. H.; Gabdrakhman.; Valiv, H.; Kainfar, E. 2021, "Nanomaterial by Sol-Gel Method: synthesis and Application". Adv. Mat. Sci. Eng. 2021, 21.

[23] Oumezzine, M.; Pena, O.; Guizouarn, T.; Lebullenger, R.; Oumezzine, M., 2012, "Impact of the sintering temperature on the structural, magnetic, and electrical transport properties of doped La0.67Ba0.33Mn0.9Cr0.1O3 manganite". J Magn Magn Mater, 324, pp.2821-2828.
[24] Rosic, M.; Kljaljevic, L.; Jordanov, D.; Stoiljikovic, M.; Kusigerski, V.; Spasojevic, V.; Matovic, B., 2015, "Effects of sintering on the structural, microstructural, and magnetic properties of nanoparticles manganite Ca1-x GdxMnO3 (x = 0.05,0.1,0.15,0.2)", Ceram Int. 41, pp. 14964-14972.

[25] Li, Y., Xue, L., Fan, L., Yan, Y., 2009, "The effect of citric acid to metal nitrates molar ratio on sol–gel combustion synthesis of nanocrystalline LaMnO3 powders", Journal of Alloys and Compounds. 478(1-2), pp. 493-497.

[26] Prabhu, Y.T., Rao, K.V., Kumar, V.S.S., Kumari, B.S., 2014, "X-Ray Analysis by Williamson-Hall and Size-Strain Plot Methods of ZnO Nanoparticles with Fuel Variation", World J. Nano Sci. and Eng., 4, 21-28.

[27] Pathan, H.M., Desai, J.D., Lokhande, C.D., 2002, "Modified Chemical Deposition and Physico- Chemical Properties of Copper Sulphide (Cu2S) Thin Films". Applied Surface Scienc, 202, pp.47-56.

[28] Srivastava, M., Ojha, A. K., Chaubey, S., Materny, A., 2009, "Synthesis and Optical Characterization of Nanocrystalline NiFe2O4 Structures". J Alloy Compd. 481, pp. 515-519.

[29] Kayani, Z.N., Manzoor, F., Zafar, A. et al. 2020, "Impact of Ag doping on structural, optical, morphological, optical and photoluminescent properties of ZnO nanoparticles". Opt Quant Electron 52, 344.

[30] Xue, S.W., Zu, X. T., Zhou, W. L., Deng, H., Xiang, X., Zhang, L., 2008, "Deng, H. Effects of Post- Thermal Annealing on the Optical Constants of ZnO Thin Films". J Alloy Compd. 448, 21-26.

[31] Greenaway, D.L., Habeke, G., 1968, "Optical and Band Structure of Semiconductors", Pergamon, New York.

[32] Guneri, E., Kariper, A., 2012, "Optical Properties of Amorphous CuS Thin Films Depositeed Chemically at Different pH values". 2012, J Alloy Compd., 516, pp.20-26.

[33] Kumar, U., Yadav. D., Upadhyay, S., 2020, "Invesigation of structural, optical, and magnetic properties of Nd-doped Sr_2SnO_4 Ruddlesden Popper oxide". J.Am.Ceram. 103, pp.05743-5757.

[34] J. F. Eloy, "Power Lasers", National School of Physics, Grenoble, France, JohnWiley & Sons (1984) 59.